

# **AGU Advances**

# <del>,</del>

## RESEARCH ARTICLE

10.1029/2025AV001785

**Peer Review** The peer review history for this article is available as a PDF in the Supporting Information.

#### **Key Points:**

- On the Barents Shelf, uppermost Permian and Lower Triassic sedimentary rocks record peak C<sub>33</sub>-n-alkylcyclohexane and phytanyl toluene contents
- C<sub>33</sub>-n-alkylcyclohexane from phytoplankton indicates blooms of certain primary producers during the Permian–Triassic environmental crisis
- Phytanyl toluene and C<sub>33</sub>-n-alkylcyclohexane may be derived from organisms occupying a similar ecological niche

#### **Supporting Information:**

Supporting Information may be found in the online version of this article.

#### Correspondence to:

S. Z. Buchwald, stella.buchwald@uni-hamburg.de

#### Citation:

Buchwald, S. Z., Birgel, D., Senger, K., Mosociova, T., Pei, Y., Zuchuat, V., et al. (2025). Phytoplankton blooms on the Barents Shelf, Svalbard, associated with the Permian–Triassic mass extinction. *AGU Advances*, 6, e2025AV001785. https://doi.org/10.1029/2025AV001785

Received 15 APR 2025 Accepted 27 SEP 2025

# **Author Contributions:**

Conceptualization: S. Z. Buchwald, D. Birgel, W. J. Foster Formal analysis: S. Z. Buchwald Funding acquisition: S. Z. Buchwald, X. Wang, W. J. Foster Investigation: S. Z. Buchwald, T. Mosociova, Y. Pei, V. Zuchuat, L. G. Tarhan, A. B. Frank, F. Galasso, M. A. Gómez Correa, E. Koşun, B. Karapunar, X. Wang, E. Kustatscher, H. Prinoth, N. Lahajnar, R. Steinkrauss, W. J. Foster

© 2025. The Author(s).

This is an open access article under the terms of the Creative Commons

Attribution License, which permits use, distribution and reproduction in any medium, provided the original work is properly cited.

# Phytoplankton Blooms on the Barents Shelf, Svalbard, Associated With the Permian-Triassic Mass Extinction

S. Z. Buchwald<sup>1</sup>, D. Birgel<sup>1</sup>, K. Senger<sup>2</sup>, T. Mosociova<sup>3</sup>, Y. Pei<sup>4</sup>, V. Zuchuat<sup>5</sup>, L. G. Tarhan<sup>6</sup>, A. B. Frank<sup>1</sup>, F. Galasso<sup>1</sup>, M. A. Gómez Correa<sup>1</sup>, E. Koşun<sup>7</sup>, B. Karapunar<sup>8</sup>, X. Wang<sup>9</sup>, E. Kustatscher<sup>10</sup>, H. Prinoth<sup>11</sup>, N. Lahajnar<sup>1</sup>, R. Steinkrauss<sup>1</sup>, J. Peckmann<sup>1</sup>, and W. J. Foster<sup>1</sup>

<sup>1</sup>Department of Earth System Sciences, University of Hamburg, Hamburg, Germany, <sup>2</sup>Department of Arctic Geology, University Centre in Svalbard, Longyearbyen, Norway, <sup>3</sup>Department of Geosciences, University of Oslo, Oslo, Norway, <sup>4</sup>State Key Laboratory of Geomicrobiology and Environmental Changes, China University of Geosciences, Wuhan, China, <sup>5</sup>CSIRO Mineral Resources, Kensington, WA, Australia, <sup>6</sup>Department of Earth and Planetary Sciences, Yale University, New Haven, CT, USA, <sup>7</sup>Department of Geological Engineering, Akdeniz University, Antalya, Türkiye, <sup>8</sup>School of Earth and Environment, University of Leeds, Leeds, UK, <sup>9</sup>Institute of Sedimentary Geology, Chengdu University of Technology, Chengdu, China, <sup>10</sup>Department of Natural History, Tirolean State Museums, Hall in Tirol, Austria, <sup>11</sup>Museum Ladin Ciastel de Tor, San Martino in Badia, Italy

**Abstract** Mid- to higher-latitude shallow marine environments are suggested to serve as refugia for organisms during intervals of rapid environmental change associated with hyperthermals. To understand the role of these environments during hyperthermals, we herein investigate the Permian-Triassic environmental crisis, which led to the most severe mass extinction event in the Phanerozoic. Our analysis of siliciclastic deposits from the Boreal Ocean from Lusitaniadalen, Svalbard, reveals a distinct increase of the lipid biomarkers  $C_{33}$ -n-alkylcyclohexane ( $C_{33}$ -n-ACH) and phytanyl toluene following the extinction event. This increase does not appear to reflect facies changes. Rather, it coincides with the extinction horizon, and persists into the lowermost Triassic (Griesbachian). Our findings suggest that neither C<sub>33</sub>-n-ACH nor phytanyl toluene are linked to short periods of photic zone euxinia recorded at Lusitaniadalen, but rather are derived from a specific group of phytoplankton. This indicates that higher-latitude ecosystems may have supported regional blooms of unknown primary producers after the Permian-Triassic mass extinction, thus explaining the selective survival of some marine organisms. We also identify (albeit in lower abundance) C<sub>33</sub>-n-ACH and its pseudohomologs in northern Italy, which is the first report of n-ACHs in the tropical Tethys region across the Permian-Triassic transition outside of South China, highlighting the wide paleogeographic distribution of this biomarker. Phytanyl toluene, however, is found exclusively in deposits recording higher-latitude ecosystems, and is likely linked to organisms occupying a similar ecological niche as the source organism of C<sub>33</sub>-n-ACH in these settings.

**Plain Language Summary** Environmental changes can have detrimental effects on marine ecosystems. Studying Earth's history can help us to understand how ecosystems respond to environmental changes. The Permian–Triassic mass extinction, the biggest mass extinction in Earth's history, is linked to rapid environmental changes. Here, we analyze two molecular fossils (lipid biomarkers),  $C_{33}$ -n-alkylcyclohexane ( $C_{33}$ -n-ACH) and phytanyl toluene, that are associated with this mass extinction, from samples from different paleolatitudes and paleo-oceans. These biomarkers increase several-fold in the aftermath of the extinction in higher-latitude settings, such as Svalbard, while we detect only traces of  $C_{33}$ -n-ACH in tropical settings, if any. Although the organisms producing these biomarkers are unknown, they were likely synthesized by organisms able to survive the harsh environmental conditions during this interval of Earth's history. This is particularly true for higher-latitude ecosystems, which may have experienced less severe environmental stress, such as less extreme (though potentially greater changes in) temperatures, compared to tropical ecosystems.  $C_{33}$ -n-ACH mirrors patterns of other biomarkers indicative of increased primary productivity during the same time interval, suggesting that it could be another molecule produced by a specific group of phytoplankton. Phytanyl toluene was probably produced by different phytoplankton found in the Boreal Ocean but not the tropical locations.

BUCHWALD ET AL. 1 of 15



Resources: D. Birgel, K. Senger, E. Koşun, X. Wang, E. Kustatscher, J. Peckmann, W. J. Foster Visualization: S. Z. Buchwald, A. B. Frank

Writing – original draft: S. Z. Buchwald Writing – review & editing: D. Birgel, K. Senger, T. Mosociova, Y. Pei, V. Zuchuat, L. G. Tarhan, A. B. Frank, F. Galasso, M. A. Gómez Correa, E. Koşun, B. Karapunar, X. Wang, E. Kustatscher, H. Prinoth, N. Lahajnar, R. Steinkrauss, J. Peckmann, W. J. Foster

### 1. Introduction

Rapid environmental changes can lead to biodiversity crises and mass extinctions. To understand the response of organisms to these changes, plasticity, adaptation or range shifts of modern species or populations can be studied (e.g., Donelson et al., 2019). However, ecosystem responses are highly complex and depend on multiple factors that are challenging to fully capture through laboratory experiments. To better understand the long-term effects of rapid environmental changes on communities, past hyperthermal events can be studied, such as the Paleocene–Eocene Thermal Maximum (e.g., McInerney & Wing, 2011) and the Permian–Triassic environmental crisis; the latter triggered the most severe mass extinction in the Phanerozoic, often referred to as the Permian–Triassic mass extinction or end-Permian mass extinction (e.g., Dal Corso et al., 2022; Payne & Clapham, 2012).

During the Permian-Triassic mass extinction, ca. 252 million years ago, approximately 81% of marine species went extinct globally (Stanley, 2016), but extinction patterns and functional diversity were geographically variable (Foster & Twitchett, 2014). The mass extinction event in marine ecosystems is constrained to  $60 \pm 48$  kyr in well-dated sections in China (Burgess et al., 2014), and was accompanied by a sharp negative carbon isotope  $(\delta^{13}C)$  excursion, observed globally (Korte & Kozur, 2010). This  $\delta^{13}C$  excursion reflects a perturbation to the carbon cycle, which remained volatile for the following ca. 500 kyr before  $\delta^{13}$ C values returned to pre-extinction levels (Burgess et al., 2014). Hence, although the extinction event (i.e., elevation in extinction rates) occurred in a geologically relatively short time interval, the environmental crisis culminating in the mass extinction probably lasted much longer. A variety of environmental factors are hypothesized to have acted as extinction drivers in marine ecosystems, such as global warming (e.g., Gliwa et al., 2022; Joachimski et al., 2012; Schobben et al., 2014) and changes in temperature gradients (Sun et al., 2024), the expansion of oxygen minimum zones (e.g., Cao et al., 2009; Penn et al., 2018; Xiang et al., 2020; F. Zhang et al., 2020), and changes in nutrient cycling (Grasby et al., 2020; Sun, 2019, 2024). Several marine ecosystems are thought to have acted as refugia for marine life during the environmental crisis, such as deep-water thermal refugia (Foster et al., 2023; Godbold et al., 2017). Similarly, modern mid- to high-latitude ecosystems may provide opportunities for equatorial taxa to escape (sub-) tropical thermal stress (Poloczanska et al., 2016). Cool-water ecosystems can, therefore, exhibit characteristic community compositions during past crises. These are reflected in the geological record, for example, in the aftermath of the Permian-Triassic mass extinction, when the northwestern shelf of Pangea was characterized by a diverse ichnofauna (Beatty et al., 2008) and contained taxa that either migrated to the Boreal Ocean or whose geographic ranges contracted to this ecosystem (Foster et al., 2023; Nakrem & Mørk, 1991), thereby flattening latitudinal diversity gradients in the extinction aftermath (e.g., Beatty et al., 2008; Foster & Twitchett, 2014; Song et al., 2020; Twitchett & Barras, 2004).

While previous studies have focused particularly on biomineralizing micro- and macrofossil communities, this study exclusively investigates molecular fossils (lipid biomarkers), aiming to enhance our understanding of ecosystem responses, particularly among primary producers, to the Permian–Triassic environmental crisis. By assessing the appearance and prevalence of the molecular fossils  $C_{33}$ -n-alkylcyclohexane ( $C_{33}$ -n-ACH) and phytanyl toluene, we aim to document differences across paleolatitudes, and determine their environmental significance in different paleo-ocean basins. Our findings therefore offer new insights into the mechanisms underlying ecosystem resilience and recovery after severe environmental perturbations.

# 2. Materials and Methods

# 2.1. Geological Setting and Sample Acquisition

The molecular fossil inventories from different Permian–Triassic successions were investigated across paleo-latitudes including sites around the Tethys, with a focus on Boreal sites recorded by the sedimentary succession of Svalbard (Figure 1). These deposits are of special interest, because Svalbard has been migrating north from the equator since the Devonian, currently occupying a high-latitude position (74–81°N), whereas it was situated at a paleolatitude of approximately 50°N during the Permian–Triassic transition (Elvevold et al., 2007; Smyrak-Sikora et al., 2025). Due to its location on the Barents Shelf in the Boreal Ocean at the northern margin of Pangea, it was isolated from the warm, equatorial water of the Tethys Ocean, thus representing a relatively cold-water shallow-marine ecosystem (e.g., Beauchamp & Baud, 2002; Worsley, 2008) contrasting with Permian–Triassic sections recording tropical settings in the Paleo- and Neotethys (Figure 1a). In the west of the main island of Svalbard's archipelago, Spitsbergen, the strata are tilted, folded and thrusted in the West Spitsbergen Fold and Thrust Belt (Dallmann et al., 1993), which represents a more proximal part of the shelf at that time (Mørk

BUCHWALD ET AL. 2 of 15

**Figure 1.** Sample locations. (a) Paleogeographic reconstruction of continental configuration at the Permian/Triassic boundary (map modified from Blakey, 2012). Yellow: sections studied here and summary of the findings (number of samples in parentheses after the section's name, and number of samples in which a compound was found is given); *n*-ACH—*n*-alkylcyclohexane; phyt—phytanyl toluene; blue: C<sub>33</sub>-*n*-ACH findings from other studies (Svalbard: Grotheer et al., 2017; Nabbefeld et al., 2010; East Greenland and Australia: Grice et al., 2005; Hays et al., 2012; South China: Saito et al., 2022; Xie et al., 2017). (b) Sampling locations on Spitsbergen, Svalbard (Base map projection: WGS 84/Arctic Polar Sterogeographic); 1: Lusitaniadalen; 2: Ledalen; 3: Høgskulefjellet; 4: Kongressfjellet; 5: Selmaneset; 6: Festningen (Vardebukta); 7: Starostinaksla; 8: Bravaisberget; 9: Reinodden. Green: C<sub>33</sub>-*n*-ACH and pseudohomologs detected; yellow: only pseudohomologs of C<sub>33</sub>-*n*-ACH detected; red point next to (1): Deltadalen.

et al., 1982). In contrast, the Permian–Triassic sedimentary successions in the more distal part of the shelf in central Spitsbergen are horizontally bedded and have undergone only small to moderate thermal alteration (Olaussen et al., 2025).

A key section for studying the Permian–Triassic transition from multiple perspectives is Lusitaniadalen (Figure 1b). The Kapp Starostin Formation and the lowermost overlying Vikinghøgda Formation record the Changhsingian, whereas most of the Vikinghøgda Formation represents the Early Triassic (Mørk et al., 1999; Zuchuat et al., 2020). We place the Kapp Starostin/Vikinghøgda formation boundary according to the definition by Nagy et al. (2025) on top of the last glauconitic sandstone bed. Due to the scarcity of macro- and microfossils in uppermost Kapp Starostin Formation, the extinction horizon at Lusitaniadalen was previously determined based on the absence of complex bioturbation in strata overlying the last glauconitic sandstone bed (Foster et al., 2023; Nabbefeld et al., 2010; Uchman et al., 2016). The transition from the last glauconitic sandstone to the very finegrained sandstones of the Vikinghøgda Formation also records an abrupt negative organic carbon isotope excursion at Lusitaniadalen (Nabbefeld et al., 2010), that has been observed globally to coincide with the extinction event (e.g., Cao et al., 2009; Sephton et al., 2005; Xie et al., 2007). The Permian/Triassic boundary, however, is not well-constrained in Lusitaniadalen, but in Deltadalen, the adjacent valley to the east (Figure 1b), it is placed approximately 2.40 m above the last glauconitic sandstone bed based on a tephra layer dated to 252.13 ± 0.62 Ma, deposited just above the local First Appearance Datum of the conodont *Hindeodus parvus* (Zuchuat et al., 2020).

Thirty-two samples were collected at Lusitaniadalen, Svalbard, from the succession of alternating bioturbated mudstones and silica-rich fine-grained sandstones (-41.51 to -30.58 m below the formation boundary) and from the uppermost glauconitic sandstone beds (-0.86 to -0.23 m) of the Kapp Starostin Formation prior to the extinction, as well as from the overlying laminated siltstones and very fine-grained sandstones from the post-extinction interval of the Vikinghøgda Formation (0.51-29.70 m), in which abundant concretionary horizons can be found. Samples were collected from unweathered outcrop exposures and wrapped in aluminum foil to avoid contamination. In particular, we focused on intervals of the Kapp Starostin Formation below the glauconitic sandstones, as the bioturbated mudstones deposited here represent conditions prior to the Permian-Triassic environmental crisis, but are lithologically comparable to the lowermost Vikinghøgda Formation. This enabled us to better account for a potential bias in the biomarker inventory introduced by the lithological change at the extinction horizon. In addition to Lusitaniadalen, eight other sections in western and central Spitsbergen were sampled to identify regional patterns in biomarker signals (Figure 1b). Lastly, we compared data from Spitsbergen with results from Tethyan sections, including data from northern Italy (western Paleotethys), the Great

BUCHWALD ET AL. 3 of 15

Bank of Guizhou in South China (eastern Paleotethys), and the Taurus Mountains in Türkiye (western Neotethys) (Figure 1a). These tropical sections are predominantly carbonate successions with thick microbialites formed in the post-extinction interval in Türkiye and South China. A more detailed description of the geological setting in northern Italy (Broglio Loriga et al., 1990; Farabegoli et al., 2007; Groves et al., 2007; Horacek et al., 2010; Massari et al., 1994; Noé, 1987; Posenato, 2010; Prinoth & Posenato, 2023), South China (Foster et al., 2018, 2019; Lehrmann et al., 1998, 2001, 2003, 2005, 2007; Payne et al., 2006), and Türkiye (Altiner & Zaninetti, 1980; Angiolini et al., 2007; Baud et al., 2005, 2007; Crasquin-Soleau et al., 2002, 2004; Lys & Marcoux, 1978; Marcoux & Baud, 1988; Özgül, 1984, 1997; Richoz, 2006; Şahin & Altiner, 2019; Stampfli et al., 1991) can be found in Supporting Information S1.

### 2.2. Sample Preparation and Data Processing

We analyzed molecular fossils from both carbonate (23 samples) and siliciclastic (66 samples) settings. To extract molecular fossils from carbonates (the majority of the samples from the Tethys), the surfaces were cut off and samples were cleaned three times with acetone to remove any contaminants from the surfaces prior to being dissolved by slowly pouring 10% hydrochloric acid onto approximately 1 cm<sup>3</sup>-sized pieces following the procedure by Birgel et al. (2006). The siliciclastic samples were cleaned with acetone and then manually powdered in an agate mortar. The total lipid extract was retrieved by extracting the samples four times with dichloromethane: methanol (3:1, v:v) for 15 min in an ultrasonic bath, and separate them into maltenes (n-hexane soluble fraction) and asphaltenes (n-hexane insoluble fraction). The maltene fraction was further separated by polarity (fractions F1-F4) using solid-phase column chromatography with a NH<sub>2</sub>-modified silica gel column (Birgel & Peckmann, 2008). The hydrocarbons (F1) were predominantly composed of n-alkanes. For a better identification and quantification of the two compounds of interest ( $C_{33}$ -n-ACH and phytanyl toluene), the n-alkanes were removed from the hydrocarbons with a molecular sieve (pore size of 5 Å), following the procedure described by Sabino et al. (2021). The compounds of interest were identified using coupled gas chromatography-mass spectrometry (GC-MS; Thermo Scientific Trace Ultra GC and Thermo Scientific DSQ II MS), searching for m/z = 83 and m/z = 106 for identification of C<sub>33</sub>-n-ACH and phytanyl toluene, respectively (Figure 2), and comparison with published spectra (McIldowie & Alexander, 2005). The aromatic hydrocarbon fraction (F2) was also scanned for phytanyl toluene, but it was not detected. For quantification, hydrocarbons were measured on a gas chromatograph coupled to a flame ionization detector (GC-FID; Thermo Scientific Trace 1310 GC). Quantification was achieved using Chromeleon 7 (version 7.2.10; Thermo Fisher Dionex) by calculating compound quantity in relation to  $5\alpha(H)$ -cholestane, the co-injection standard, and normalizing it to the sample's TOC content. For TOC determination (Figure S1 in Supporting Information S1), samples were de-carbonated with 100 μL 1M HCl and analyzed with a Euro EA 3000 (Euro Vector) elemental analyzer with a precision of ±0.05% and standard deviations <0.08. C<sub>33</sub>-n-ACH and phytanyl toluene could only be quantified in samples from Lusitaniadalen. In other sections both targeted compounds either co-elute with other compounds or their content was too low to be quantified. Where only trace amounts were identified, only the presence or absence is reported. Correlations between the content of biomarkers were determined with the software R (version 4.3.2) (2023). The maturity of the samples was estimated with the methylphenanthrene index (MPI) after Cassani et al. (1988) by using the peak areas of 1-, 2-, 3- and 9-methylphenanthrene (MP) from m/z = 192, and phenanthrene (P) from m/z = 178 in the mass chromatogram of the F2 fraction, following MPI = 1.89(2-MP + 3-MP)/[P + 1.26(1-MP + 9-MP)]. Due to incomplete chromatographic separation, a proportion of phenanthrene and the methylphenanthrenes often coeluted in the F1 fraction. However, a recalculation of the MPI from the F1 fraction revealed that methylphenanthrene and phenanthrene co-eluted proportionally, and the general pattern per region (central Svalbard, western Svalbard, northern Italy, South China, Türkiye) is preserved (Figure S2 in Supporting Information S1).

## 3. Results and Discussion

# 3.1. Occurrence and Paleogeographic Distribution of C33-n-Alkylcyclohexane and Phytanyl Toluene

The content of  $C_{33}$ -n-ACH in samples from Lusitaniadalen, Svalbard, shows a more than ten-fold increase from 8.1 to 43.3  $\mu$ g/g TOC in the pre-extinction samples to values up to 513.5  $\mu$ g/g TOC right above the extinction horizon (Figure 3a). Although the pre-extinction samples may have experienced stronger microbial degradation than post-extinction samples as indicated by the larger hump of the unresolved complex mixture (UCM; Figure 2), the signal of increased post-extinction abundance of  $C_{33}$ -n-ACH is also preserved in the ratio of  $C_{33}$ -n-ACH and n- $C_{34}$  (Figure S1 in Supporting Information S1). Since n-ACHs are more resistant to biodegradation

BUCHWALD ET AL. 4 of 15

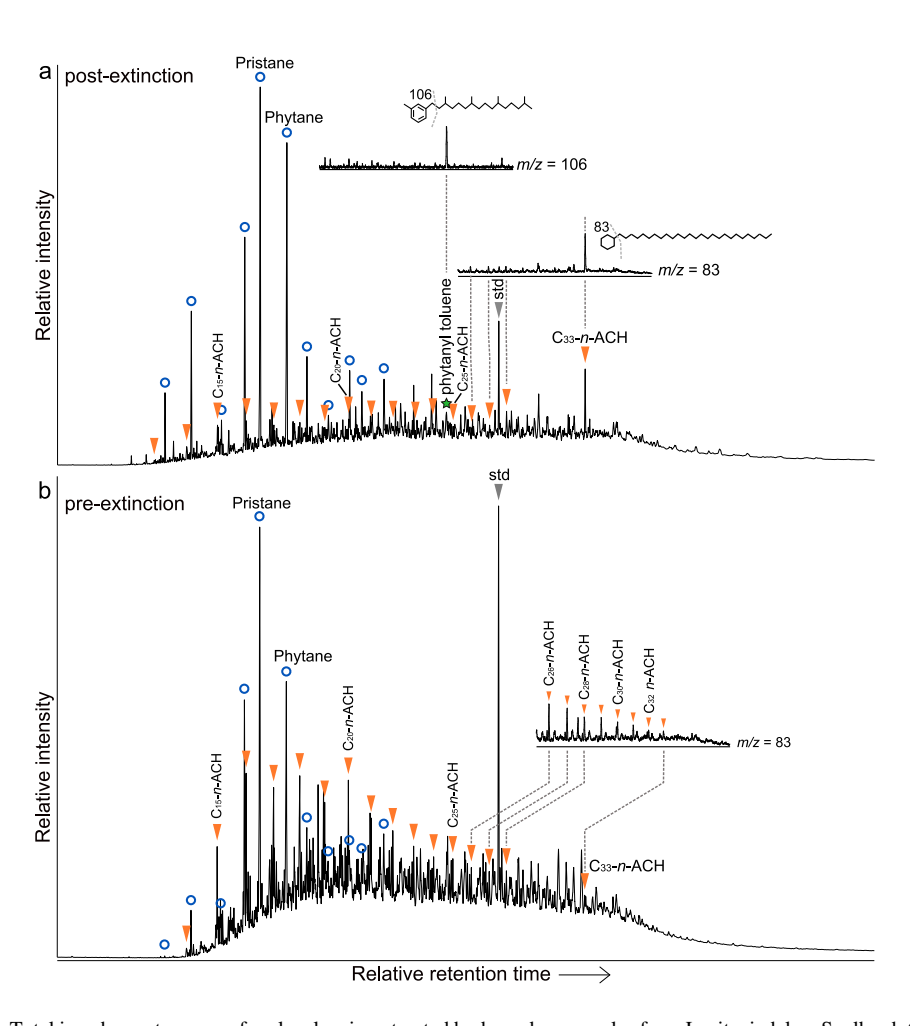


Figure 2. Total ion chromatograms of molecular sieve-treated hydrocarbon samples from Lusitaniadalen, Svalbard. (a) Post-extinction: 0.51 m above the extinction horizon; (b) pre-extinction: -36.87 m below the extinction horizon; orange triangles:  $C_{33}$ -n-alkylcyclohexane ( $C_{33}$ -n-ACH) and its pseudohomologs; green star: phytanyl toluene; blue circles: pseudohomologous series of head-to-tail linked  $C_{15-25}$ -isoprenoids; gray triangle:  $5\alpha(H)$ -cholestane standard (std). The mass ranges of m/z = 83 to scan for  $C_{33}$ -n-ACH and its pseudohomologs and m/z = 106 to scan for phytanyl toluene are shown.

than n-alkanes (Koma et al., 2003; Perry & Gibson, 1977), the higher post-extinction ratios cannot be attributed to differential degradation, but instead point to a genuine increase in C<sub>33</sub>-n-ACH. The content of C<sub>33</sub>-n-ACH within the first 30 m above the extinction horizon remains elevated, which indicates persistently favorable environmental conditions for the producers of C<sub>33</sub>-n-ACH or its unknown precursor molecule during the Permian-Triassic environmental crisis. Furthermore, n-ACHs with shorter (<C<sub>33</sub>) alkyl-chains are detected, and show a similar sharp increase in abundance from 156.0 to 710.7 μg/g TOC (sum of C<sub>14-28</sub>-n-ACH) before the environmental crisis to up to 4,948 µg/g TOC above the extinction horizon (Figure 3b). Similar to the early diagenetic shortening of the alkyl-chains of acyclic isoprenoids (Moldowan & Seifert, 1979) and hopanoids (Rohmer et al., 1980), microbial activity and early diagenetic fragmentation may result in a series of pseudohomolog n-ACHs (Luo et al., 2013; Saito et al., 2022), that derived from the same precursor. We find a strong correlation between C<sub>33</sub>-n-ACH and shorter-chain  $C_{14-28}$ -n-ACH above the extinction horizon (correlation coefficient r = 0.73-0.97, Figure S3 in Supporting Information S1). However, correlations are generally weaker between  $C_{33}$ -n-ACH and  $C_{18-28}$ -n-ACH (correlation coefficient r = 0.60-0.83), and insignificant for  $C_{14-17}$ -n-ACH below the extinction horizon (Figure S3 in Supporting Information S1). The strong correlation above the extinction horizon suggests that  $C_{14-28}$ -n-ACH are degradation products and pseudohomologs of  $C_{33}$ -n-ACH. The weaker correlations below the extinction horizon suggest that an additional source of n-ACHs potentially contributed to the n-ACH pool, such as degraded fatty acids (e.g., Rubinstein & Strausz, 1979; Shimoyama & Johns, 1972). Also, post-depositional carbon chain elongation may have contributed minor amounts of n-ACHs originating from shorter-chain fatty acids, although shortening of the carbon chain is the dominant reaction during diagenesis and thermal maturation,

BUCHWALD ET AL. 5 of 15

and carbon chain elongation has never been observed for alkyl-chains longer than  $C_{28}$  (Shimoyama & Johns, 1972). However, even in pre-crisis samples where both  $C_{33}$ -n-ACH and shorter-chain n-ACHs are detected, a proportion of these shorter-chain n-ACHs are likely pseudohomologs of  $C_{33}$ -n-ACH. This implies that the absence of  $C_{33}$ -n-ACH does not necessarily indicate that the source organism(s) were absent, but may suggest enhanced degradation of the precursor molecule for instances in which shorter n-ACHs are present.

Phytanyl toluene is absent in the samples taken from horizons preceding the onset of the Permian–Triassic environmental crisis, except for the last sample below the extinction horizon at -0.23 m with 75.9  $\mu$ g/g TOC (Figure 3c). Above the extinction horizon at Lusitaniadalen, phytanyl toluene occurs with a maximum content of 425.4  $\mu$ g/g TOC in the lowest post-extinction sample at 0.51 m. Its content varies but, except for the sample at 13.73 m, remains elevated throughout the section between 12.2 and 216.0  $\mu$ g/g TOC, thereby resembling the Lower Triassic C<sub>33</sub>-n-ACH content (correlation coefficient r = 0.75, Figure S3 in Supporting Information S1).

The occurrence of C33-n-ACH and its pseudohomologs at Lusitaniadalen is not restricted to samples above the extinction horizon; it also occurs in uppermost Permian pre-crisis samples. Compared to previous studies on lipid biomarkers at Lusitaniadalen (Grotheer et al., 2017; Nabbefeld et al., 2010), this study provides a temporally extended record of the Lusitaniadalen profile. This extended record into the Lower Triassic possibly accounts for the differences in the absolute content of post-extinction  $C_{33}$ -n-ACH compared to that reported by Nabbefeld et al. (2010; Figure S4 in Supporting Information S1), who may have captured only the onset of the increase in the content of this biomarker. Additionally, the extended sampling range of our study allows for the establishment of a pre-extinction biomarker base line, and a decoupling of biotic from abiotic (e.g., facies-related) effects on the biomarker inventory, such as a lithological control on biomarker preservation (Peters, 1986; Peters et al., 2005), and the actual biotic change by comparing the C33-n-ACH and phytanyl toluene content below and above the extinction horizon from similar lithologies and depositional environments. Previously reported content changes of C<sub>33</sub>-n-ACH and phytanyl toluene across the extinction horizon at Lusitaniadalen were limited to the glauconitic sandstones for the pre-crisis signal (Grotheer et al., 2017; Nabbefeld et al., 2010), raising the possibility that the reported changes may have resulted from lithological rather than environmental change. Our new data clearly support that lithology was not the main control on the C<sub>33</sub>-n-ACH and phytanyl toluene content. Instead, the source organism(s) of C<sub>33</sub>-n-ACH showed resilience to the significant environmental perturbations across the

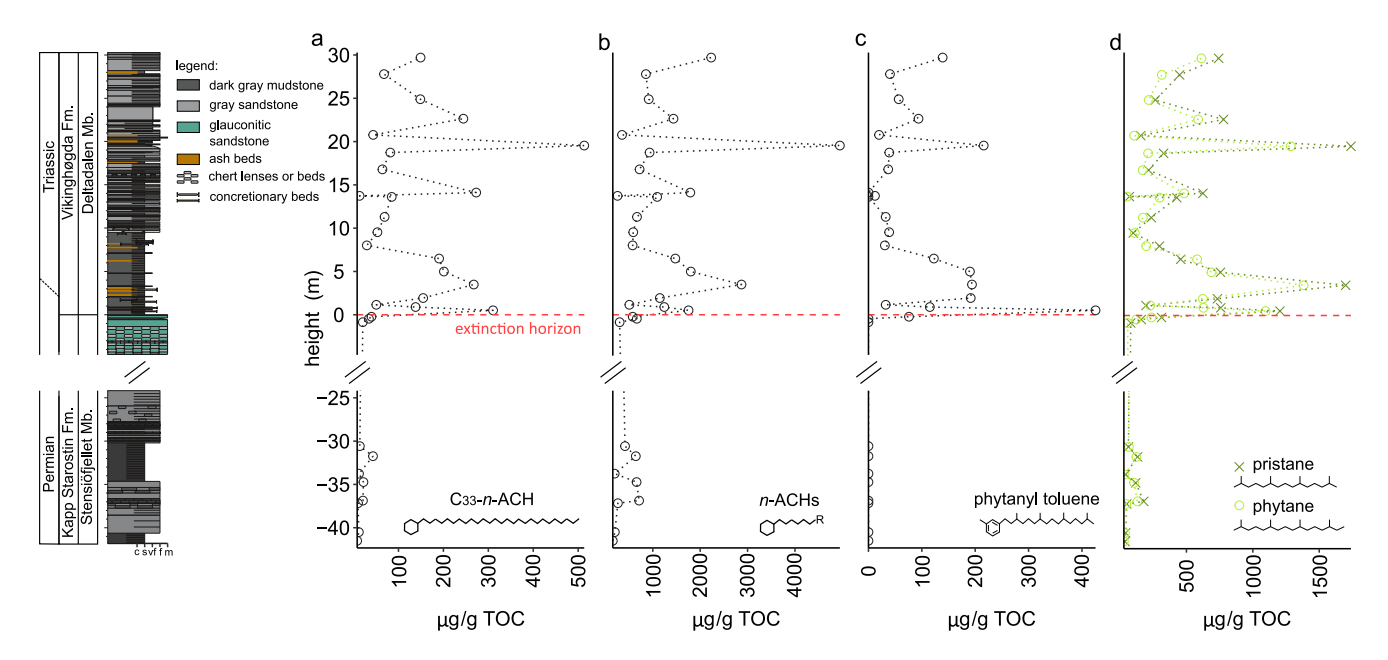


Figure 3. Biomarker profiles across the siliciclastic Permian–Triassic succession at Lusitaniadalen, Svalbard. (a) content of  $C_{33}$ -n-alkylcyclohexane ( $C_{33}$ -n-ACH); (b) sum of the content of shorter-chain pseudohomologs of  $C_{33}$ -n-ACH ( $C_{14-28}$ -n-ACH quantified;  $C_{29-32}$ -n-ACH are present in the samples but co-elute with other compounds, and cannot be quantified); (c) content of phytanyl toluene; (d) content of pristane (head-to-tail linked  $C_{19}$ -isoprenoid) and phytane (head-to-tail linked  $C_{20}$ -isoprenoid). The red dashed line marks the extinction horizon (Foster et al., 2023; Nabbefeld et al., 2010; Uchman et al., 2016). Note that the y-axis is broken (as indicated by parallel diagonal line segments) to focus on sampling intervals; similar pre- and post-extinction lithologies were targeted to control for potential lithofacies bias on the biomarker data. c—claystone; s—siltstone; vf—very fine-grained sandstone; f—fine-grained sandstone; m—medium-grained sandstone.

BUCHWALD ET AL. 6 of 15

257 6604x, 2025, 5, Downloaded from https://agupubs.onlinelibrary.wiley.com/doi/10.1029/2025AV001785 by NICE, National

Institute for Health and Care Excellence, Wiley Online Library on [24/10/2025]. See the T

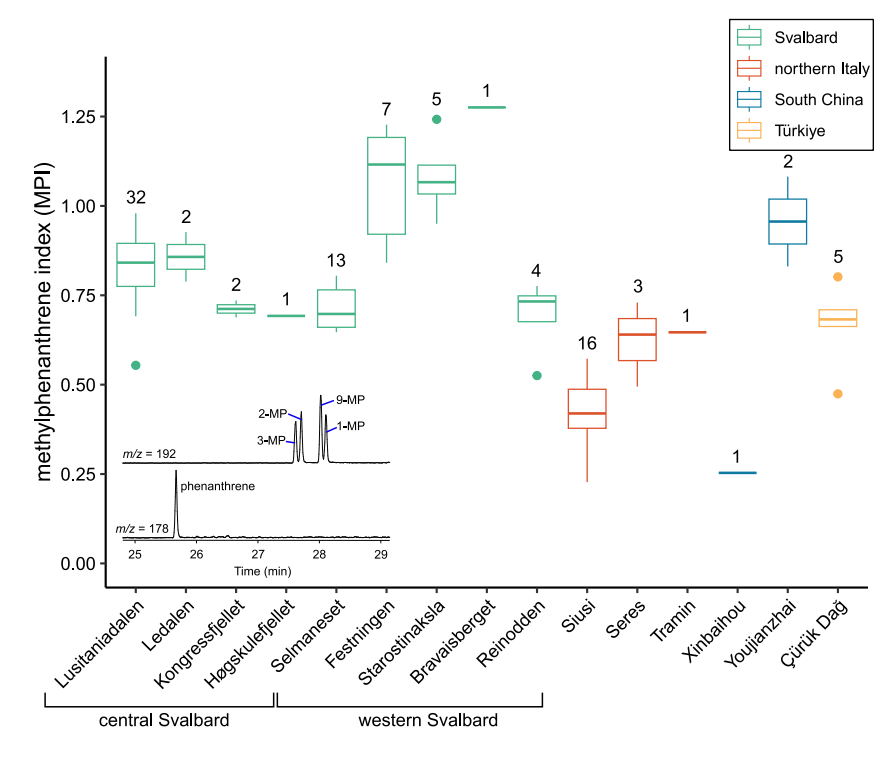


Figure 4. Methylphenanthrene index (MPI) for an estimation of thermal maturity across all investigated sections. The numbers on the boxes denote the total number of analyzed samples per section that contained all compounds required to calculate the MPI. MPI = 1.89(2-MP + 3-MP)/[P + 1.26(1-MP + 9-MP)]; MP = peak area of methylphenanthrene from m/z = 192 mass chromatogram; P = peak area of phenanthrene from m/z = 178 mass chromatogram (see inserted example of mass chromatograms).

Permian/Triassic boundary, and the source organisms of both  $C_{33}$ -n-ACH and phytanyl toluene thrived in the post-extinction ecosystem.

C<sub>33</sub>-n-ACH and its pseudohomologs were not only detected in Lusitaniadalen, but also in other Permian-Triassic sites from central Spitsbergen, including Kongressfjellet and Høgskulefjellet, and in the Olenekian at Ledalen (Figure 1b). From western Spitsbergen, at Starostinaksla and Festningen (Figure 1b), C<sub>33</sub>-n-ACH is only detected above the extinction horizon, but pseudohomologs are nonetheless abundant in underlying strata prior to the environmental crisis. Three other western Spitsbergen sections (Reinodden, Bravaisberget, Selmaneset) contain only trace amounts of pseudohomologs that are commonly co-eluted with other compounds in the molecular sieve-treated samples. The apparently enhanced preservation of  $C_{33}$ -n-ACH in central Spitsbergen compared to western Spitsbergen is likely caused by the lower maturity of the material in central Spitsbergen. In the western Spitsbergen sections, enhanced tectonic activity during the formation of the West Spitsbergen Fold and Thrust Belt in the Eocene (Braathen et al., 1999; Leever et al., 2011; Saalmann & Thiedig, 2001) led to higher temperature and pressure, which in turn increased maturity and the degradation of sedimentary organic molecules (cf. Peters et al., 2005). As the methylphenantrene index (MPI) exhibits a non-linear relationship with thermal maturity with a maximum MPI at a vitrinite reflectance  $(R_o)$  of 1.35% (Boreham et al., 1988; Radke & Welte, 1983), we infer that the lower MPI in samples from central Spitsbergen, compared to the higher MPI in western Spitsbergen sites reflects thermally less mature material (Figure 4). Except for an outlier at 13.73 m, the MPI at Lusitaniadalen is within a relatively narrow range (MPI = 0.69-0.98; Figure S1 in Supporting Information S1), indicating a similar thermal history across the section. However, as the shorter-chain n-ACHs are likely derived from the degradation of C<sub>33</sub>-n-ACH (especially above the extinction horizon), the source organism(s) appear to have thrived across a range of depositional environments from the more distal area in central Spitsbergen to the more proximal area in western Spitsbergen (Mørk et al., 1982). Phytanyl toluene, however, was detected in samples from all sites in central Spitsbergen (Lusitaniadalen, Kongressfjellet, Høgskulefjellet, Ledalen; Figure 1b), but could not be detected in western Spitsbergen samples. This absence may

BUCHWALD ET AL. 7 of 15

suggest greater susceptibility to degradation during maturation of the host lithologies, or the exclusion of the source organism(s) from the more proximal part of the basin.

The increased content of  $C_{33}$ -n-ACH above the extinction horizon agrees with previous findings, primarily from temperate settings like Western Australia and East Greenland (Grice et al., 2005; Hays et al., 2012) and earlier work from Svalbard (Grotheer et al., 2017; Nabbefeld et al., 2010). In contrast, phytanyl toluene was less frequently recognized across the Permian/Triassic boundary than  $C_{33}$ -n-ACH. It has thus far been detected in sections cropping out in Svalbard, Western Australia and East Greenland, whereas it is absent in sites recording lower-paleolatitude ecosystems like the Meishan section in South China (Cao et al., 2009; Grotheer et al., 2017) and other tropical settings in the Tethys Ocean investigated in this study. Both compounds, therefore, represent valuable geochemical markers of the Permian–Triassic environmental crisis and the Early Triassic in higher-latitude ecosystems. However, the distinctly high abundance of the  $C_{33}$ -n-ACH homolog seems to be restricted to Permian–Triassic successions, whereas phytanyl toluene is less temporally restricted and has also been recognized from deposits formed during other geological intervals (e.g., Jurassic: Plet et al., 2020; Cretaceous: Moura et al., 2019; Neogene: Sinninghe Damsté et al., 1993).

Existing reports of  $C_{33}$ -n-ACH in paleo-(sub)tropical ecosystems are restricted to South China (Shangsi section: Xie et al., 2017; Chaohu section: Saito et al., 2022). In this study, pseudohomologs of  $C_{33}$ -n-ACH in South China were only found in samples from Youjianzhai (Figure 1a). However, the thermal maturity of the organic matter at Youjianzhai is rather high (mean MPI = 0.96), and methylphenanthrenes were only present in one of the samples from Xinbaihou, the second section in South China (Figure 4). These samples may record a post-mature signal, also reflected in the very low MPI of 0.25 of the sample from Xinbaihou. While neither  $C_{33}$ -n-ACH nor n-ACHs were recorded across the Permian/Triassic boundary in the Taurus Mountains in Türkiye, we detected pseudohomologs of  $C_{33}$ -n-ACH and minor traces of  $C_{33}$ -n-ACH in pre-extinction samples from northern Italy, which is the first report of late Permian n-ACHs in the Tethys region outside South China. However, contents were too low for quantification and the pseudohomologs commonly co-elute with other compounds.  $C_{33}$ -n-ACH has only been quantified in the Tethys region at Shangsi, with an increase from 0  $\mu$ g/g TOC prior to the Permian–Triassic environmental crisis to up to 35.08  $\mu$ g/g TOC above the extinction event (Xie et al., 2017). This post-extinction content at Shangsi is within the same order of magnitude as the pre-crisis content at Lusitaniadalen. Although no pseudohomologs are reported from Shangsi accounting for degraded  $C_{33}$ -n-ACH, the low  $C_{33}$ -n-ACH content suggests less favorable conditions for the source organism(s) to proliferate at this equatorial site.

While the studied sections from the Boreal Ocean are exclusively siliciclastic successions, the Tethys sections analyzed for  $C_{33}$ -n-ACH and phytanyl toluene are carbonate-dominated deposits. Carbonate and clastic systems vary in their pore water chemistry, cementation or sedimentation rate and adsorption of organic matter to minerals, which might affect the preservation of organic compounds (e.g., Hemingway et al., 2019; Peters et al., 2005). Hence, a depositional control on the preservation of biomolecules cannot be excluded. To fully understand factors controlling the geographic variability in both  $C_{33}$ -n-ACH and phytanyl toluene content, their abundance needs to be constrained in tropical siliciclastic deposits such as the Bódvaszilas Sandstone Formation in Hungary (Hips, 1996) or the Yinkeng Formation in Meishan, South China (Yin et al., 2001).

# 3.2. Potential Sources of the Extinction Markers

Although the absolute content of  $C_{33}$ -n-ACH and its pseudohomologs is several-fold smaller in the tropical Tethys region compared to the Boreal Ocean and higher-latitude regions, an increase of this biomarker after the onset of the Permian–Triassic environmental crisis can be globally observed, but its source organism(s) remain enigmatic. Dong et al. (1993) suggested that n-ACHs were formed by cyclization of long-chain (> $C_{25}$ ) fatty acids during diagenesis. Long-chain fatty acids and n-alkanes are important components of leaf waxes of land plants (Buschhaus & Jetter, 2011), and would therefore imply terrestrial plant material as the source of long-chain n-ACHs. In such a case, the n-ACHs would originate from the same precursor molecules as n-alkanes with the same carbon number, which would be reflected in a similar carbon number distribution of n-ACHs and n-alkanes. However, unlike  $C_{33}$ -n-ACH, the n- $C_{33}$  alkane does not record peak abundances compared to other n-alkanes above the extinction horizon (Figures S1 and S5 in Supporting Information S1). A terrestrial plant source is therefore unlikely.

Others have suggested a phytoplankton source of  $C_{33}$ -n-ACH, as its content shows a similar stratigraphic trend to that of the chlorophyll-derived biomarkers pristane and phytane, although the absolute contents differ (Nabbefeld

BUCHWALD ET AL. 8 of 15

et al., 2010), as well as increased abundance of the spinose acritarch genera Michrystridium and Veryhachium at the onset of the  $C_{33}$ -n-ACH increase (Grice et al., 2005). In addition,  $C_{33}$ -n-ACH exhibits a similar  $\delta^{13}$ C composition as phytane with -33.4% and -32.7%, respectively (Grice et al., 2005). At Lusitaniadalen, strong correlations between the content of pristane and  $C_{33}$ -n-ACH (correlation coefficient r = 0.91; Figure S3 in Supporting Information S1) and between phytane and  $C_{33}$ -n-ACH (correlation coefficient r = 0.90; Figure S3 in Supporting Information S1) are recorded. Both pristane and phytane contents increase several fold from 28.8 to 312.3 µg/g TOC prior to the environmental crisis to 1,204 µg/g TOC and 1,096 µg/g TOC, respectively, immediately above the extinction horizon (Figure 3d). Notably, the highest pre-crisis content of pristane and phytane at Lusitaniadalen is recorded in the penultimate glauconitic sandstone bed at -0.23 m below the extinction horizon. This aligns with the lowermost detection of phytanyl toluene in the same bed, indicating a gradual increase in the presence of the source organism(s) of phytanyl toluene, rather than an abrupt onset. In addition to chlorophyll and algal tocopherols, pristane and phytane can also derive from the degradation of archaeal isoprenoid compounds (Rontani & Bonin, 2011; Rowland, 1990). Indeed, head-to-tail linked isoprenoid pseudohomologs from  $C_{21}$  up to  $C_{25}$  were detected in the samples (Figure 2), potentially representing degradation products of extended archaeol (Vandier et al., 2021). However, the abundance of pristane and phytane strongly exceeds the usual ratios of phytanyl to sesterterpanyl-chains in archaea producing extended archaeol in seawater (cf. Vandier et al., 2021) (Figure 2). This suggests that the majority of pristane and phytane in our samples can be interpreted as derived from phototrophic source organisms rather than from the degradation of membrane lipids of archaea, which might only partially contribute to the total pristane and phytane pools.

Additionally, the source organism(s) of C<sub>33</sub>-n-ACH have been previously assumed to be associated with euxinic conditions, based on increased content of green sulfur bacteria-derived biomarkers, aryl isoprenoids, which indicate photic zone euxinia within two meters across the extinction horizon at Lusitaniadalen (Nabbefeld et al., 2010). Instead of anoxygenic green sulfur bacteria, we suggest oxygenic phytoplankton as the source of C<sub>33</sub>-n-ACH, particularly in the post-extinction interval at Lusitaniadalen. This interpretation is supported by the diverse pelagic and benthic fauna, including radiolarians, sponges, bivalves, gastropods, brachiopods and ammonoids, preserved in the basal Vikinghøgda Formation (Foster et al., 2017, 2023). The presence of these aerobic, heterotrophic organisms excludes persistent anoxic or euxinic conditions in either the water column or bottom waters at Lusitaniadalen. Furthermore, redox conditions reconstructed from independent geochemical proxies indicate that the persistence of anoxic and euxinic conditions in Svalbard was comparatively short-lived; these signals disappear approximately 10 m above the extinction horizon (Grasby et al., 2015; Zuchuat et al., 2020). In contrast, both C<sub>33</sub>-n-ACH and phytanyl toluene contents generally remain elevated throughout the investigated interval up to 30 m above the extinction horizon, indicating the source organism(s) were able to grow in oxygenated water. Nonetheless, waxing and waning of photic zone euxinia could have been an important control during the environmental crisis, and the aryl isoprenoids detected by Nabbefeld et al. (2010) as well as variability in extents and styles of burrowing (Rodríguez-Tovar et al., 2021) could indicate intermittent pulses of oxygen stress. Even during episodes of expanding euxinia, oxygenic phototrophs could have persisted and bloomed in an oxygenated surface water layer (e.g., Kasprak et al., 2015; Słowakiewicz et al., 2015). Enhanced remobilization of phosphorus from the seafloor during euxinic or anoxic periods during the Permian-Triassic environmental crisis in Svalbard (Schobben et al., 2020) could have provided otherwise limited nutrients that fertilized phytoplankton blooms. With specific (albeit of unknown affinity) photoautotrophic primary producers able to cope with and even thrive under Early Triassic environmental conditions, blooms of these organisms may have helped sustain planktic food webs and the comparatively less depauperate benthic communities recorded in the Svalbard fossil record (Foster et al., 2017, 2023) through sufficient organic carbon export to the seafloor. Yet, the small size of benthic species and large number of premature and larval shells also suggest that the environmental crisis persisted into the Griesbachian, preventing full ecological recovery.

A change in the composition of primary producers and an increased flux of marine algal material to the sediment, potentially indicating increased primary productivity, was also recognized across the extinction event in the Canadian Sverdrup basin (Algeo et al., 2012). In contrast, in South China, in sections recording a tropical setting, and in which we found  $C_{33}$ -n-ACH and phytanyl toluene to be less abundant or absent, an abrupt decline in primary productivity was observed right before the onset of the extinction (Y. Zhang et al., 2018). A follow-up meta-analysis has identified this decline as a potential factor explaining the severe loss of biodiversity during the Permian–Triassic environmental crisis (Foster et al., 2024). Hence, primary productivity was likely geographically variable across a range of paleolatitudinal settings (Algeo et al., 2013). Productivity and the community

BUCHWALD ET AL. 9 of 15

composition of primary producers are influenced by diverse factors, such as nutrient availability, growth temperature, depth of the photic zone, or oxidant availability, as shown by studies of modern primary productivity (e.g., Arrigo, 2005; Domingues & Barbosa, 2023; Grimaud et al., 2017; Pajares & Ramos, 2019; Wong et al., 2023). An interplay of these factors likely also affected the phototrophic community across the Permian-Triassic transition (e.g., Algeo et al., 2012; Grasby et al., 2016, 2019; Schobben et al., 2020; Shen et al., 2015). Factors such as global warming likely played a role in shaping the phototrophic community composition and gross primary productivity during the Permian-Triassic environmental crisis (e.g., Gliwa et al., 2022; Joachimski et al., 2012), but regional factors must also be considered. For example, terrestrial erosion has been proposed to have increased during the Permian-Triassic environmental crisis in the Paleotethys (Sephton et al., 2005; Wu et al., 2023) and a large delta plain developed on the Early Triassic Barents Shelf, discharging massive amounts of terrestrial material to the shelf (Eide et al., 2018; Gilmullina et al., 2022). Although these terrestrial inputs could provide an important nutrient source and may fertilize phytoplankton (e.g., Putland et al., 2014), increased turbidity may have alternatively impeded increased productivity or led to changes in the primary producer community composition (e.g., Domingues & Barbosa, 2023). Hence, changes in past productivity remain challenging to reconstruct, due to a paucity of direct proxy records and dependence on the complex interplay of many factors. Thus, although a phytoplankton bloom is indicated in the Boreal Realm at Svalbard, we cannot directly infer a local change in primary productivity. However, the post-extinction increases of the chlorophyll-derived biomarkers pristane and phytane as well as relatively diverse higher trophic levels suggest that regional primary productivity was maintained, if not even promoted.

While the tropical Tethys Ocean may have experienced a decrease in primary productivity (Algeo et al., 2013; Y. Zhang et al., 2018), tropical carbonate successions are often characterized by the formation of microbialites (e.g., Foster et al., 2020; Kershaw et al., 2012). These have been attributed to a cyanobacterial origin, for example, in Türkiye, Iran (Heindel et al., 2018) and South China (Xie et al., 2010), which suggests benthic microbial mats contributed to primary production. Neither  $C_{33}$ -n-ACH nor phytanyl toluene have been previously reported from these Lower Triassic microbialites in Türkyie, Iran, and South China, but shorter-chain n-ACHs have been detected at Cili, South China, by Luo et al. (2013), who found distinctly elevated relative abundances of  $C_{21}$ -n-ACH compared to  $C_{20}$ -n-ACH. Furthermore, an increase of characteristic cyanobacterial biomarkers such as n- $C_{17}$  compared to other n-alkanes, or mono-, di- and trimethylated alkanes (e.g., Coates et al., 2014; Gelpi et al., 1970; Heindel et al., 2018; Plet et al., 2020) was not found in samples with increased contents of  $C_{33}$ -n-ACH or phytanyl toluene (this study). Consequently, a cyanobacterial source of  $C_{33}$ -n-ACH and phytanyl toluene is unlikely.

The source organism(s) of phytanyl toluene remains enigmatic. Phytanyl benzenes were previously hypothesized to originate from diagenetically altered carotenoids (Gallegos, 1981; Grotheer et al., 2017; Summons & Powell, 1987) or isoprenoid quinones (Sinninghe Damsté et al., 1988). In the case of phytanyl toluene, this would suggest a defunctionalized and demethylated benzoquinone (an isoprenoid quinone with a single benzene ring) as a potential precursor molecule. However, quinones are ubiquitous across the domains of life, especially in archaea and bacteria (Collins & Jones, 1981), but also in eukaryotes (Nowicka & Kruk, 2010). The strong correlation of phytanyl toluene and C<sub>33</sub>-n-ACH observed at Lusitaniadalen supports that both compounds derived from organisms with similar ecological requirements. However, phytanyl toluene is absent throughout most of the investigated interval prior to the environmental crisis whereas C<sub>33</sub>-n-ACH was detected in pre-extinction strata at selected sites, which suggests that although the source organisms of phytanyl toluene and C<sub>33</sub>-n-ACH were likely different, they may have occupied a similar ecological niche during the Permian–Triassic environmental crisis. Both compounds were most likely derived from phototrophic algae.

# 4. Conclusions

The biomarker data for  $C_{33}$ -n-ACH and phytanyl toluene presented here extend their record in Svalbard temporally and spatially, enabling the decoupling of lithological change at the extinction horizon from changes in the biomarker inventory. The increased content of both biomarkers above the extinction horizon is interpreted as a response to the Permian–Triassic environmental crisis rather than being driven by changes in the depositional environment. However, their preservation is likely substantially influenced by enhanced degradation at thermally more altered sites, underscoring the importance for careful evaluation when biomarkers are absent. Our findings challenge the previous hypothesis that the source organism(s) of  $C_{33}$ -n-ACH are associated with photic zone euxinia as we found no evidence of extended euxinic conditions during the whole interval of increased  $C_{33}$ -n-

BUCHWALD ET AL. 10 of 15

doi/10.1029/2025AV001785 by NICE,

ACH content. Instead,  $C_{33}$ -n-ACH was likely produced during blooms of specific planktonic oxygenic phototrophs in the Boreal Ocean and at higher paleolatitudes in the Early Triassic, potentially forming the base of a resilient ecological community, reflected in the diverse Early Triassic fossil assemblage in Svalbard. Phytanyl toluene, exclusively observed in higher paleolatitude siliciclastic successions and absent in tropical carbonate deposits, appears to have a different source than  $C_{33}$ -n-ACH. The spatial disparity in their paleogeographic distribution may reflect differences in environmental requirements, depositional settings, or the distribution of their source organism(s).

### **Conflict of Interest**

The authors declare no conflicts of interest relevant to this study.

# **Data Availability Statement**

The biomarker data, metadata and R code used in the study are available at Zenodo (Buchwald et al., 2025: https://www.doi.org/10.5281/zenodo.16032548).

## References

- Algeo, T. J., Henderson, C. M., Ellwood, B., Rowe, H., Elswick, E., Bates, S., et al. (2012). Evidence for a diachronous late Permian marine crisis from the Canadian Arctic region. GSA Bulletin, 124(9–10), 1424–1448. https://doi.org/10.1130/B30505.1
- Algeo, T. J., Henderson, C. M., Tong, J., Feng, Q., Yin, H., & Tyson, R. V. (2013). Plankton and productivity during the Permian–Triassic boundary crisis: An analysis of organic carbon fluxes. Global and Planetary Change, 105, 52–67. https://doi.org/10.1016/j.gloplacha.2012. 02.008
- Altiner, D., & Zaninetti, L. (1980). Le Trias dans la région de Pinarbasi, Taurus oriental, Turquie: Unités lithologiques, micropaléontologie, milieux de dépôt. Rivista Italiana di Paleontologia e Stratigrafia, 86(4), 705–760.
- Angiolini, L., Carabelli, L., Nicora, A., Crasquin-Soleau, S., Marcoux, J., & Rettori, R. (2007). Brachiopods and other fossils from the Permo—Triassic boundary beds of the Antalya Nappes (SW Taurus, Turkey). Geobios, 40(6), 715–729. https://doi.org/10.1016/j.geobios.2007.01.007
  Arrigo, K. R. (2005). Marine microorganisms and global nutrient cycles. Nature, 437(7057), 349–355. https://doi.org/10.1038/nature04159
- Baud, A., Richoz, S., & Marcoux, J. (2005). Calcimicrobial cap rocks from the basal Triassic units: Western Taurus occurrences (SW Turkey). Comptes Rendus Palevol, 4(6–7), 569–582. https://doi.org/10.1016/j.crpv.2005.03.001
- Baud, A., Richoz, S., & Pruss, S. (2007). The lower Triassic anachronistic carbonate facies in space and time. *Global and Planetary Change*, 55(1–3), 81–89. https://doi.org/10.1016/j.gloplacha.2006.06.008
- Beatty, T. W., Zonneveld, J. P., & Henderson, C. M. (2008). Anomalously diverse Early Triassic ichnofossil assemblages in northwest Pangea: A case for a shallow-marine habitable zone. *Geology*, 36(10), 771–774. https://doi.org/10.1130/G24952A.1
- Beauchamp, B., & Baud, A. (2002). Growth and demise of Permian biogenic chert along northwest Pangea: Evidence for end-Permian collapse of thermohaline circulation. *Palaeogeography, Palaeoclimatology, Palaeoecology, 184*(1–2), 37–63. https://doi.org/10.1016/S0031-0182(02)
- Birgel, D., & Peckmann, J. (2008). Aerobic methanotrophy at ancient marine methane seeps: A synthesis. *Organic Geochemistry*, 39(12), 1659–1667. https://doi.org/10.1016/j.orggeochem.2008.01.023
- Birgel, D., Thiel, V., Hinrichs, K.-U., Elvert, M., Campbell, K. A., Reitner, J., et al. (2006). Lipid biomarker patterns of methane-seep microbialites from the Mesozoic convergent margin of California. *Organic Geochemistry*, 37(10), 1289–1302. https://doi.org/10.1016/j.orggeochem. 2006 02 004
- Blakey, R. (2012). Global paleogeography. Retrieved from http://www2.nau.edu/rcb7/globaltext2.html
- Boreham, C. J., Crick, I. H., & Powell, T. G. (1988). Alternative calibration of the Methylphenanthrene Index against vitrinite reflectance: Application to maturity measurements on oils and sediments. *Organic Geochemistry*, 12(3), 289–294. https://doi.org/10.1016/0146-6380(88)
- Braathen, A., Bergh, S. G., & Maher, H. D., Jr. (1999). Application of a critical wedge taper model to the Tertiary transpressional fold-thrust belt on Spitsbergen, Svalbard. GSA Bulletin, 111(10), 1468–1485. https://doi.org/10.1130/0016-7606(1999)111<1468:AOACWT>2.3.CO;2
- Broglio Loriga, C., Góczán, F., Haas, J., Lenner, K., Neri, C., Oravecz Scheffer, A., et al. (1990). The lower Triassic sequences of the Dolomites (Italy) and Transdanubian Mid-Mountains (Hungary) and their correlation. *Memorie di Scienze Geologiche*, 11(2), 41–103.
- Buchwald, S. Z., Birgel, D., Senger, K., Mosociova, T., Pei, Y., Zuchuat, V., et al. (2025). Phytoplankton blooms on the Barents Shelf, Svalbard, associated with the Permian–Triassic mass extinction. StellaZBuchwald/Permian-Triassic\_Extinction\_Markers [Dataset Computational Notebook]. Zenodo. https://www.doi.org/10.5281/zenodo.16032548
- Burgess, S. D., Bowring, S., & Shen, S. Z. (2014). High-precision timeline for Earth's most severe extinction. *Proceedings of the National Academy of Sciences of the United States of America*, 111(9), 3316–3321. https://doi.org/10.1073/pnas.1317692111
- Buschhaus, C., & Jetter, R. (2011). Composition differences between epicuticular and intracuticular wax substructures: How do plants seal their epidermal surfaces? *Journal of Experimental Botany*, 62(3), 841–853. https://doi.org/10.1093/jxb/erq366
- Cao, C., Love, G. D., Hays, L. E., Wang, W., Shen, S., & Summons, R. E. (2009). Biogeochemical evidence for euxinic oceans and ecological disturbance presaging the end-Permian mass extinction event. *Earth and Planetary Science Letters*, 281(3–4), 188–201. https://doi.org/10. 1016/j.epsl.2009.02.012
- Cassani, F., Gallango, O., Talukdar, S., Vallejos, C., & Ehrmann, U. (1988). Methylphenanthrene maturity index of marine source rock extracts and crude oils from the Maracaibo Basin. Organic Geochemistry, 13(3), 73–80. https://doi.org/10.1016/B978-0-08-037236-5.50013-0
- Coates, R. C., Podell, S., Korobeynikov, A., Lapidus, A., Pevzner, P., Sherman, D. H., et al. (2014). Characterization of cyanobacterial hydrocarbon composition and distribution of biosynthetic pathways. *PLoS One*, 9(1), e85140. https://doi.org/10.1371/journal.pone.0085140
- Collins, M. D., & Jones, D. (1981). Distribution of isoprenoid quinone structural types in bacteria and their taxonomic implications. *Microbiological Reviews*, 45(2), 316–354. https://doi.org/10.1128/mr.45.2.316-354.1981

Acknowledgments

We acknowledge the logistical support from the Czech Arctic Research Station including RV Clione and its crew David Vostárek and Jiří Štojdl jr, the crew of Ulla Rinman Mana Walther, Jan Walther, and Karlis Baltacs, as well as UNIS, and the Governor of Svalbard for granting us sampling permission (permit No. 23/ 00910-2 and 24/00386-4). Also, we would like to thank everyone who helped us in planning and conducting fieldwork in Svalbard, northern Italy, South China and Türkiye for their support and guidance, and Sabine Beckmann for her support in the lab. We are grateful for the thoughtful and constructive comments of three reviewers. This research was funded by two Arctic Field Grants from the Research Council of Norway (Project No. 342069 and 250229) and the Deutsche Forschungsgemeinschaft (Project No. FO1297/1-1). Fieldwork in South China was funded by the National Natural Science Foundation of China (Project No. 42293291, 42102143). We also acknowledge financial support from the Open Access Publication Fund of the University of Hamburg, Open Access funding enabled and organized by Projekt DEAL.

BUCHWALD ET AL. 11 of 15

- Crasquin-Soleau, S., Marcoux, J., Angiolini, L., Richoz, S., Nicora, A., Baud, A., & Bertho, Y. (2004). A new ostracode fauna from the Permian-Triassic boundary in Turkey (Taurus, Antalya Nappes). *Micropaleontology*, 50(3), 281–295. https://doi.org/10.2113/50.3.281
- Crasquin-Soleau, S., Richoz, S., Marcoux, J., Angiolini, L., Nicora, A., & Baud, A. (2002). Les événements de la limite Permien–Trias: Derniers survivants et/ou premiers re-colonisateurs parmi les ostracodes du Taurus (Sud-Ouest de la Turquie). *Comptes Rendus Geoscience*, 334(7), 489–495. https://doi.org/10.1016/S1631-0713(02)01782-0
- Dal Corso, J., Song, H., Callegaro, S., Chu, D., Sun, Y., Hilton, J., et al. (2022). Environmental crises at the Permian–Triassic mass extinction. Nature Reviews Earth & Environment, 3(3), 197–214. https://doi.org/10.1038/s43017-021-00259-4
- Dallmann, W. K., Andresen, A., Bergh, S., Maher, H. D., Jr., & Ohta, Y. (1993). Tertiary fold-and-thrust belt of Spitsbergen, Svalbard. In Norsk Polarinstitutt Meddelelser (Vol. 128).
- Domingues, R. B., & Barbosa, A. B. (2023). Evaluating underwater light availability for phytoplankton: Mean light intensity in the mixed layer versus attenuation coefficient. *Water*, 15(16), 2966. https://doi.org/10.3390/w15162966
- Donelson, J. M., Sunday, J. M., Figueira, W. F., Gaitán-Espitia, J. D., Hobday, A. J., Johnson, C. R., et al. (2019). Understanding interactions between plasticity, adaptation and range shifts in response to marine environmental change. *Philosophical Transactions of the Royal Society B*, 374(1768), 20180186. https://doi.org/10.1098/rstb.2018.0186
- Dong, J.-Z., Vorkink, W. P., & Lee, M. L. (1993). Origin of long-chain alkylcyclohexanes and alkylbenzenes in a coal-bed wax. Geochmica et Cosmmhimica Acta, 57(4), 837–849. https://doi.org/10.1016/0016-7037(93)90172-S
- Eide, C. H., Klausen, T. G., Katkov, D., Suslova, A. A., & Helland-Hansen, W. (2018). Linking an Early Triassic delta to antecedent topography: Source-to-sink study of the southwestern Barents Sea margin. GSA Bulletin, 130(1–2), 263–283. https://doi.org/10.1130/B31639.1
- Elvevold, S., Dallmann, W., & Blomeier, D. (2007). Geology of Svalbard. Norwegian Polar Institute.
- Farabegoli, E., Perri, M. C., & Posenato, R. (2007). Environmental and biotic changes across the Permian-Triassic boundary in western Tethys: The Bulla parastratotype, Italy. *Global and Planetary Change*, 55(1–3), 109–135. https://doi.org/10.1016/j.gloplacha.2006.06.009
- Foster, W. J., Asatryan, G., Rauzi, S., Botting, J. P., Buchwald, S. Z., Lazarus, D. B., et al. (2023). Response of siliceous marine organisms to the Permian-Triassic climate crisis based on new findings from central Spitsbergen, Svalbard. *Paleoceanography and Paleoclimatology*, 38(12), e2023PA004766. https://doi.org/10.1029/2023PA004766
- Foster, W. J., Danise, S., & Twitchett, R. J. (2017). A silicified Early Triassic marine assemblage from Svalbard. *Journal of Systematic Palaeontology*, 15(10), 851–877. https://doi.org/10.1080/14772019.2016.1245680
- Foster, W. J., Frank, A. B., Li, Q., Danise, S., Wang, X., & Peckmann, J. (2024). Thermal and nutrient stress drove Permian–Triassic shallow marine extinctions. *Cambridge Prisms: Extinction*, 2, e9. https://doi.org/10.1017/ext.2024.9
- Foster, W. J., Heindel, K., Richoz, S., Gliwa, J., Lehrmann, D. J., Baud, A., et al. (2020). Suppressed competitive exclusion enabled the proliferation of Permian/Triassic boundary microbialites. *Depositional Record*, 6(1), 62–74. https://doi.org/10.1002/dep2.97
- Foster, W. J., Lehrmann, D. J., Hirtz, J. A., White, M., Yu, M., Li, J., & Martindale, R. C. (2019). Early Triassic benthic invertebrates from the Great Bank of Guizhou, South China: Systematic palaeontology and palaeobiology. *Papers in Palaeontology*, 5(4), 613–656. https://doi.org/ 10.1002/spp2.1252
- Foster, W. J., Lehrmann, D. J., Yu, M., Ji, L., & Martindale, R. C. (2018). Persistent environmental stress delayed the recovery of marine communities in the aftermath of the latest Permian mass extinction. *Paleoceanography and Paleoclimatology*, 33(4), 338–353. https://doi.org/10.1002/2018PA003328
- Foster, W. J., & Twitchett, R. J. (2014). Functional diversity of marine ecosystems after the late Permian mass extinction event. *Nature Geoscience*, 7(3), 233–238. https://doi.org/10.1038/ngeo2079
- Gallegos, E. J. (1981). Alkylbenzenes derived from carotenes in coals by GC/MS. Journal of Chromatographic Science, 19(4), 177–182. https://doi.org/10.1093/chromsci/19.4.177
- Gelpi, E., Schneider, H., Mann, J., & Oró, J. (1970). Hydrocarbons of geochemical significance in microscopic algae. *Phytochemistry*, 9(3), 603–612. https://doi.org/10.1016/S0031-9422(00)85700-3
- Gilmullina, A., Klausen, T. G., Doré, A. G., Rossi, V. M., Suslova, A., & Eide, C. H. (2022). Linking sediment supply variations and tectonic evolution in deep time, source-to-sink systems—The Triassic Greater Barents Sea Basin. *Bulletin of the Geological Society of America*, 134(7–8), 1760–1780. https://doi.org/10.1130/B36090.1
- Gliwa, J., Wiedenbeck, M., Schobben, M., Ullmann, C. V., Kiessling, W., Ghaderi, A., et al. (2022). Gradual warming prior to the end-Permian mass extinction. *Palaeontology*, 65(5), e12621. https://doi.org/10.1111/pala.12621
- Godbold, A., Schoepfer, S., Shen, S., & Henderson, C. M. (2017). Precarious ephemeral refugia during the earliest Triassic. *Geology*, 45(7), 607–610. https://doi.org/10.1130/G38793.1
- Grasby, S. E., Beauchamp, B., Bond, D. P. G., Wignall, P., Talavera, C., Galloway, J. M., et al. (2015). Progressive environmental deterioration in northwestern Pangea leading to the latest Permian extinction. *Bulletin of the Geological Society of America*, 127(9–10), 1331–1347. https://doi.org/10.1130/B31197.1
- Grasby, S. E., Beauchamp, B., & Knies, J. (2016). Early Triassic productivity crises delayed recovery from world's worst mass extinction. Geology, 44(9), 779–782. https://doi.org/10.1130/G38141.1
- Grasby, S. E., Knies, J., Beauchamp, B., Bond, D. P., Wignall, P., & Sun, Y. (2020). Global warming leads to Early Triassic nutrient stress across northern Pangea. GSA Bulletin, 132(5–6), 943–954. https://doi.org/10.1130/B32036.1
- Grasby, S. E., Them II, T. R., Chen, Z., Yin, R., & Ardakani, O. H. (2019). Mercury as a proxy for volcanic emissions in the geologic record. Earth-Science Reviews, 196, 102880. https://doi.org/10.1016/j.earscirev.2019.102880
- Grice, K., Twitchett, R. J., Alexander, R., Foster, C. B., & Looy, C. (2005). A potential biomarker for the Permian–Triassic ecological crisis. Earth and Planetary Science Letters, 236(1–2), 315–321. https://doi.org/10.1016/j.epsl.2005.05.008
- Grimaud, G. M., Mairet, F., Sciandra, A., & Bernard, O. (2017). Modeling the temperature effect on the specific growth rate of phytoplankton: A review. Reviews in Environmental Science and Biotechnology, 16(4), 625–645. https://doi.org/10.1007/s11157-017-9443-0
- Grotheer, H., Le Métayer, P., Piggott, M. J., Lindeboom, E. J., Holman, A. I., Twitchett, R. J., & Grice, K. (2017). Occurrence and significance of phytanyl arenes across the Permian-Triassic boundary interval. *Organic Geochemistry*, 104, 42–52. https://doi.org/10.1016/j.orggeochem. 2016.12.002
- Groves, J. R., Rettori, R., Payne, J. L., Boyce, M. D., Demi, D., & Altiner, D. (2007). End-Permian mass extinction of lagenide foraminifers in the Southern Alps (northern Italy). *Journal of Paleontology*, 81(3), 415–434. https://doi.org/10.1666/05123.1
- Hays, L. E., Grice, K., Foster, C. B., & Summons, R. E. (2012). Biomarker and isotopic trends in a Permian–Triassic sedimentary section at Kap Stosch, Greenland. Organic Geochemistry, 43, 67–82. https://doi.org/10.1016/j.orggeochem.2011.10.010
- Heindel, K., Foster, W. J., Richoz, S., Birgel, D., Roden, V. J., Baud, A., et al. (2018). The formation of microbial-metazoan bioherms and biostromes following the latest Permian mass extinction. *Gondwana Research*, 61, 187–202. https://doi.org/10.1016/j.gr.2018.05.007

BUCHWALD ET AL. 12 of 15

- Hemingway, J. D., Rothman, D. H., Grant, K. E., Rosengard, S. Z., Eglinton, T. I., Derry, L. A., & Galy, V. V. (2019). Mineral protection regulates long-term global preservation of natural organic carbon. *Nature*, 570(7760), 228–231. https://doi.org/10.1038/s41586-019-1280-6
- Hips, K. (1996). Stratigraphic and facies evaluation of the Lower Triassic formations in the Aggtelek-Rudabánya Mountains, NE Hungary. Acta Geologica Hungarica, 39(4), 369–411.
- Horacek, M., Povoden, E., Richoz, S., & Brandner, R. (2010). High-resolution carbon isotope changes, litho- and magnetostratigraphy across Permian-Triassic boundary sections in the Dolomites, N-Italy. New constraints for global correlation. *Palaeogeography, Palaeoclimatology, Palaeoecology*, 290(1–4), 58–64. https://doi.org/10.1016/j.palaeo.2010.01.007
- Joachimski, M. M., Lai, X., Shen, S., Jiang, H., Luo, G., Chen, B., et al. (2012). Climate warming in the latest Permian and the Permian-Triassic mass extinction. Geology, 40(3), 195–198. https://doi.org/10.1130/G32707.1
- Kasprak, A. H., Sepúlveda, J., Price-Waldman, R., Williford, K. H., Schoepfer, S. D., Haggart, J. W., et al. (2015). Episodic photic zone euxinia in the northeastern Panthalassic Ocean during the end-Triassic extinction. *Geology*, 43(4), 307–310. https://doi.org/10.1130/G36371.1
- Kershaw, S., Crasquin, S., Li, Y., Collin, P. Y., Forel, M. B., Mu, X., et al. (2012). Microbialites and global environmental change across the Permian–Triassic boundary: A synthesis. *Geobiology*, 10(1), 25–47. https://doi.org/10.1111/j.1472-4669.2011.00302.x
- Koma, D., Hasumi, F., Chung, S. Y., & Kubo, M. (2003). Biodegradation of n-alkylcyclohexanes by co-oxidation via multiple pathways in Acinetobacter sp. ODDK71. Journal of Bioscience and Bioengineering, 95(6), 641–644. https://doi.org/10.1016/S1389-1723(03)80178-0
- Korte, C., & Kozur, H. W. (2010). Carbon-isotope stratigraphy across the Permian–Triassic boundary: A review. *Journal of Asian Earth Sciences*, 39(4), 215–235. https://doi.org/10.1016/j.jseaes.2010.01.005
- Leever, K. A., Gabrielsen, R. H., Faleide, J. I., & Braathen, A. (2011). A transpressional origin for the West Spitsbergen fold-and-thrust belt: Insight from analog modeling. *Tectonics*, 30(2), TC2014. https://doi.org/10.1029/2010TC002753
- Lehrmann, D. J., Enos, P., Payne, J. L., Montgomery, P., Wei, J., Yu, Y., et al. (2005). Permian and Triassic depositional history of the Yangtze platform and Great Bank of Guizhou in the Nanpanijang basin of Guizhou and Guangxi, south China. *Albertiana*, 33(1), 149–168.
- Lehrmann, D. J., Jiayong, W., & Enos, P. (1998). Controls on facies architecture of a large Triassic carbonate platform; the Great Bank of Guizhou, Nanpanjiang Basin, South China. *Journal of Sedimentary Research*, 68(2), 311–326. https://doi.org/10.2110/jsr.68.311
- Lehrmann, D. J., Payne, J. L., Felix, S. V., Dillett, P. M., Wang, H., Yu, Y., & Wei, J. (2003). Permian–Triassic boundary sections from shallow-marine carbonate platforms of the Nanpanjiang Basin, South China: Implications for oceanic conditions associated with the end-Permian extinction and its aftermath. *PALAIOS*, 18(2), 138–152. https://doi.org/10.1669/0883-1351(2003)18<138:PBSFSC>2.0.CO;2
- Lehrmann, D. J., Payne, J. L., Pei, D., Enos, P., Druke, D., Steffen, K., et al. (2007). Record of the end-Permian extinction and Triassic biotic recovery in the Chongzuo-Pingguo platform, southern Nanpanjiang basin, Guangxi, south China. *Palaeogeography, Palaeoclimatology, Palaeoecology*, 252(1–2), 200–217. https://doi.org/10.1016/j.palaeo.2006.11.044
- Lehrmann, D. J., Wan, Y., Wei, J., Yu, Y., & Xiao, J. (2001). Lower Triassic peritidal cyclic limestone: An example of anachronistic carbonate facies from the Great Bank of Guizhou, Nanpanjiang Basin, Guizhou province, South China. *Palaeogeography, Palaeoclimatology, Palaeoecology*, 173(3–4), 103–123. https://doi.org/10.1016/S0031-0182(01)00302-9
- Luo, G., Wang, Y., Grice, K., Kershaw, S., Algeo, T. J., Ruan, X., et al. (2013). Microbial-algal community changes during the latest Permian ecological crisis: Evidence from lipid biomarkers at Cili, South China. Global and Planetary Change, 105, 36–51. https://doi.org/10.1016/j.gloplacha.2012.11.015
- Lys, M., & Marcoux, J. (1978). Les niveaux du Permien supérieurdes Nappes d'Antalya (Taurides occidentales, Turquie). Comptes Rendus de l'Académie des Sciences, 286, 1417–1420.
- Marcoux, J., & Baud, A. (1988). The Permo-Triassic boundary in the Antalya Nappes (Western Taurides-Turkey). Memoir Società Geologica Italiana, 34, 243–252.
- Massari, F., Neri, C., Pittau, P., Fontana, D., & Stefani, C. (1994). Sedimentology, palynostratigraphy and sequence stratigraphy of a continental to shallow-marine rift-related succession: Upper Permian of the eastern Southern Alps (Italy). Memorie di Scienze Geologiche, 46, 119–243.
- McIldowie, M., & Alexander, R. (2005). Identification of a novel C<sub>33</sub> n-alkylcyclohexane biomarker in Permian–Triassic sediments. *Organic Geochemistry*, 36(10), 1454–1458. https://doi.org/10.1016/j.orggeochem.2005.06.009
- McInerney, F. A., & Wing, S. L. (2011). The Paleocene-Eocene thermal maximum: A perturbation of carbon cycle, climate, and biosphere with implications for the future. *Annual Review of Earth and Planetary Sciences*, 39(1), 489–516. https://doi.org/10.1146/annurev-earth-040610-133431
- Moldowan, J. M., & Seifert, W. K. (1979). Head-to-head linked isoprenoid hydrocarbons in petroleum. Science, 204(4389), 169–171. https://doi.org/10.1126/science.204.4389.169
- Mørk, A., Elvebakk, G., Forsberg, A. W., Hounslow, M. W., Nakrem, H. A., Vigran, J. O., & Weitschat, W. (1999). The type section of the Vikinghøgda formation: A new Lower Triassic unit in central and eastern Svalbard. *Polar Research*, 18(1), 51–82. https://doi.org/10.1111/j. 1751-8369 1999 tb00277 x
- Mørk, A., Knarud, R., & Worsley, D. (1982). Depositional and diagenetic environments of the Triassic and lower Jurassic successions of Svalbard. In A. F. Embry & H. R. Balkwill (Eds.), *Arctic geology and geophysics* (pp. 371–398). Canadian Society of Petroleum Geologists.
- Moura, A. K., Ribeiro, D. O., do Carmo, I. S., Araújo, B. Q., Pereira, V. B., Azevedo, D. A., & Citó, A. M. (2019). An assay on alkyl aromatic hydrocarbons: Unexpected group-type separation of diaromatic hydrocarbons in Cretaceous crude oils from Brazilian Marginal Basin. *Energy & Fuels*, 33(2), 691–699. https://doi.org/10.1021/acs.energyfuels.8b03268
- Nabbefeld, B., Grice, K., Twitchett, R. J., Summons, R. E., Hays, L., Böttcher, M. E., & Asif, M. (2010). An integrated biomarker, isotopic and palaeoenvironmental study through the late Permian event at Lusitaniadalen, Spitsbergen. *Earth and Planetary Science Letters*, 291(1–4), 84–96. https://doi.org/10.1016/j.epsl.2009.12.053
- Nagy, J., Svensen, H. H., & Planke, S. (2025). Severe oxygen and carbonate depletion during the end-Permian mass extinction and its aftermath in boreal waters reflected by Foraminifera from spitsbergen. *Preprint at SSRN*, 4460346.
- Nakrem, H. A., & Mørk, A. (1991). New early Triassic Bryozoa (Trepostomata) from Spitsbergen, with some remarks on the stratigraphy of the investigated horizons. *Geological Magazine*, 128(2), 129–140. https://doi.org/10.1017/S001675680001832X
- Noé, S. (1987). Facies and paleogeography of the marine upper Permian and of the Permian-Triassic boundary in the Southern alps (Bellerophon Formation, tesero horizon). Facies, 16, 89–142. https://doi.org/10.1007/BF02536749
- Nowicka, B., & Kruk, J. (2010). Occurrence, biosynthesis and function of isoprenoid quinones. Biochimica et Biophysica Acta Bioenergetics, 1797(9), 1587–1605. https://doi.org/10.1016/j.bbabio.2010.06.007
- Olaussen, S., Grundvåg, S.-A., Senger, K., Anell, I., Betlem, P., Birchall, T., et al. (2025). Svalbard composite tectono-sedimentary element, Barents Sea. *Geological Society*, 57(1), M57-2021. https://doi.org/10.1144/m57-2021-36
- Özgül, N. (1984). Stratigraphy and tectonic evolution of the Central Taurides. Geology of the Taurus belt. In *International symposium* (pp. 77–90). Özgül, N. (1997). Bozkır-Hadım-Taşkent (orta toroslar'in kuzey kesimi) dolayında yer alan tektono-stratigrafik birliklerin stratigrafisi. *Maden Tektik ve Arama Dergisi*, 119, 113–174.

BUCHWALD ET AL. 13 of 15

- Pajares, S., & Ramos, R. (2019). Processes and microorganisms involved in the marine nitrogen cycle: Knowledge and gaps. Frontiers in Marine Science, 6, 739. https://doi.org/10.3389/fmars.2019.00739
- Payne, J., & Clapham, M. (2012). End-Permian mass extinction in the oceans: An ancient analog for the twenty-first century? Annual Review of Earth and Planetary Sciences, 40(1), 89–111. https://doi.org/10.1146/annurev-earth-042711-105329
- Payne, J. L., Lehrmann, D. J., Wei, J., & Knoll, A. H. (2006). The pattern and timing of biotic recovery from the end-Permian extinction on the Great Bank of Guizhou, Guizhou Province, China. PALAIOS, 21(1), 63–85. https://doi.org/10.2110/palo.2005.p05-12p
- Penn, J. L., Deutsch, C., Payne, J. L., & Sperling, E. A. (2018). Temperature-dependent hypoxia explains biogeography and severity of end-Permian marine mass extinction. *Science*, 362(6419), eaat1327. https://doi.org/10.1126/science.aat1327
- Perry, J. J., & Gibson, D. T. (1977). Microbial metabolism of cyclic hydrocarbons and related compounds. CRC Critical Reviews in Microbiology, 5(4), 387–412. https://doi.org/10.3109/10408417709102811
- Peters, K. E. (1986). Guidelines for evaluating petroleum source rock using programmed pyrolysis. AAPG Bulletin, 70(3), 318–329. https://doi.org/10.1306/94885688-1704-11D7-8645000102C1865D
- Peters, K. E., Walters, C. C., & Moldowan, J. M. (2005). The Biomarker Guide: Volume 1, Biomarkers and isotopes in the environment and human history (2nd ed., Vol. 1). Cambridge University Press.
- Plet, C., Grice, K., Scarlett, A. G., Ruebsam, W., Holman, A. I., & Schwark, L. (2020). Aromatic hydrocarbons provide new insight into carbonate concretion formation and the impact of eogenesis on organic matter. *Organic Geochemistry*, 143, 103961. https://doi.org/10.1016/j. orggeochem.2019.103961
- Poloczanska, E. S., Burrows, M. T., Brown, C. J., Molinos, J. G., Halpern, B. S., Hoegh-Guldberg, O., et al. (2016). Responses of marine organisms to climate change across oceans. Frontiers in Marine Science, 3, 62, https://doi.org/10.3389/fmars.2016.00062
- Posenato, R. (2010). Marine biotic events in the Lopingian succession and latest Permian extinction in the Southern Alps (Italy). *Geological Journal*, 45(2–3), 195–215, https://doi.org/10.1002/gi.1212
- Prinoth, H., & Posenato, R. (2023). Bivalves from the Changhsingian (upper Permian) Bellerophon Formation of the Dolomites (Italy): Ancestors of Lower Triassic post-extinction benthic communities. *Papers in Palaeontology*, 9(2), e1486. https://doi.org/10.1002/spp2.1486
- Putland, J. N., Mortazavi, B., Iverson, R. L., & Wise, S. W. (2014). Phytoplankton biomass and composition in a river-dominated estuary during
- two summers of contrasting river discharge. *Estuaries and Coasts*, 37(3), 664–679. https://doi.org/10.1007/s12237-013-9712-2 Radke, M., & Welte, D. H. (1983). The Methylphenanthrene Index (MPI): A maturity parameter based on aromatic hydrocarbons. In M. Bjoroy
- (Ed.), Advances in organic geochemistry (pp. 504–512). Wiley.

  R Core Team. (2023). R: A Language and environment for statistical computing. R Foundation for Statistical Computing. Retrieved from https://
- www.R-project.org/
  Richoz, S. (2006). Stratigraphie isotopique du Permien superieur et Trias inferieur de quelques localites de la Neotethys. *Memoire de Geologie*
- (Lausanne), 46, 283.

  Rodríguez-Toyar F. I. Dorador I. Zuchuat V. Planke S. & Hammer Ø (2021) Response of macrobenthic trace maker community to the end-
- Rodríguez-Tovar, F. J., Dorador, J., Zuchuat, V., Planke, S., & Hammer, Ø. (2021). Response of macrobenthic trace maker community to the end-Permian mass extinction in Central Spitsbergen, Svalbard. *Palaeogeography, Palaeoclimatology, Palaeoecology*, 581, 110637. https://doi.org/ 10.1016/j.palaeo.2021.110637
- Rohmer, M., Dastillung, M., & Ourisson, G. (1980). Hopanoids from C<sub>30</sub> to C<sub>35</sub> in recent muds: Chemical markers for bacterial activity. Naturwissenschaften, 67(9), 456–458. https://doi.org/10.1007/BF00405643
- Rontani, J. F., & Bonin, P. (2011). Production of pristane and phytane in the marine environment: Role of prokaryotes. *Research in Microbiology*, 162(9), 923–933. https://doi.org/10.1016/j.resmic.2011.01.012
- Rowland, S. J. (1990). Production of acyclic isoprenoid hydrocarbons by laboratory maturation of methanogenic bacteria. *Organic Geochemistry*, 15(15), 9–16. https://doi.org/10.1016/0146-6380(90)90181-X
- Rubinstein, I., & Strausz, O. P. (1979). Geochemistry of the thiourea adduct fraction from Alberta petroleum. *Geochimica et Cosmochimica Acta*, 43(8), 1387–1392. https://doi.org/10.1016/0016-7037(79)90129-7
- Saalmann, K., & Thiedig, F. (2001). Tertiary West Spitsbergen fold and thrust belt on Brøggerhalvøya, Svalbard: Structural evolution and kinematics. *Tectonics*, 20(6), 976–998. https://doi.org/10.1029/2001TC900016
- Sabino, M., Dela Pierre, F., Natalicchio, M., Birgel, D., Gier, S., & Peckmann, J. (2021). The response of water column and sedimentary environments to the advent of the Messinian salinity crisis: Insights from an onshore deep-water section (Govone, NW Italy). *Geological Magazine*, 158(5), 825–841. https://doi.org/10.1017/S0016756820000874
- Şahin, N., & Altiner, D. (2019). Testing of Permian–Lower Triassic stratigraphic data in a half-Graben/tilt-block system: Evidence for the initial rifting phase in Antalya Nappes. Canadian Journal of Earth Sciences, 56(11), 1262–1283. https://doi.org/10.1139/cjes-2018-0169
- Saito, R., Tian, L., Kaiho, K., & Takahashi, S. (2022). Biomarker evidence for the prolongation of multiple phytoplankton blooms in the aftermath of the end-Permian mass extinction. *Palaeogeography, Palaeoclimatology, Palaeoecology*, 600, 111077. https://doi.org/10.1016/j.palaeo. 2022.111077
- Schobben, M., Foster, W. J., Sleveland, A. R. N., Zuchuat, V., Svensen, H. H., Planke, S., et al. (2020). A nutrient control on marine anoxia during the end-Permian mass extinction. *Nature Geoscience*, 13(9), 640–646. https://doi.org/10.1038/s41561-020-0622-1
- Schobben, M., Joachimski, M. M., Korn, D., Leda, L., & Korte, C. (2014). Palaeotethys seawater temperature rise and an intensified hydrological cycle following the end-Permian mass extinction. *Gondwana Research*, 26(2), 675–683. https://doi.org/10.1016/j.gr.2013.07.019
- Sephton, M. A., Looy, C. V., Brinkhuis, H., Wignall, P. B., de Leeuw, J. W., & Visscher, H. (2005). Catastrophic soil erosion during the end-Permian biotic crisis. *Geology*, 33(12), 941–944. https://doi.org/10.1130/G21784.1
- Shen, J., Schoepfer, S. D., Feng, Q., Zhou, L., Yu, J., Song, H., et al. (2015). Marine productivity changes during the end-Permian crisis and Early Triassic recovery. *Earth-Science Reviews*, 149, 136–162. https://doi.org/10.1016/j.earscirev.2014.11.002
- Shimoyama, A., & Johns, W. D. (1972). Formation of alkenes from fatty acids in the presence of CaCO3. *Geochimica et Cosmochimica Acta*, 36(1), 87–91. https://doi.org/10.1016/0016-7037(72)90122-6
- Sinninghe Damsté, J. S., Keely, B. J., Betts, S. E., Baas, M., Maxwell, J. R., & de Leeuw, J. W. (1993). Variations in abundances and distributions of isoprenoid chromans and long-chain alkylbenzenes in sediments of the Mulhouse Basin: A molecular sedimentary record of palaeosalinity. Organic Geochemistry, 20(8), 1201–1215. https://doi.org/10.1016/0146-6380(93)90009-Z
- Sinninghe Damsté, J. S., Kock-van Dalen, A. C., & De Leeuw, J. W. (1988). Identification of long-chain isoprenoid alkylbenzenes in sediments and crude oils. *Geochimica et Cosmochimica Acta*, 52(11), 2671–2677. https://doi.org/10.1016/0016-7037(88)90035-X
- Słowakiewicz, M., Tucker, M. E., Perri, E., & Pancost, R. D. (2015). Nearshore euxinia in the photic zone of an ancient sea. *Palaeogeography*, *Palaeoclimatology*, *Palaeoecology*, 426, 242–259. https://doi.org/10.1016/j.palaeo.2015.03.022
- Smyrak-Sikora, A., Betlem, P., Engelschiøn, V. S., Foster, W. J., Grundvåg, S.-A., Jelby, M. E., et al. (2025). *Phanerozoic paleoenvironmental and paleoclimatic evolution in Svalbard* (pp. 2024–3912). Preprint EGUsphere. https://doi.org/10.5194/egusphere-2024-3912

BUCHWALD ET AL. 14 of 15

, 2025, 5, Downloadec

.1029/2025AV001785 by NICE,

- Song, H., Huang, S., Jia, E., Dai, X., Wignall, P. B., & Dunhill, A. M. (2020). Flat latitudinal diversity gradient caused by the Permian–Triassic mass extinction. *Proceedings of the National Academy of Sciences*, 117(30), 17578–17583. https://doi.org/10.1073/pnas.1918953117
- Stampfli, G., Marcoux, J., & Baud, A. (1991). Tethyan margins in space and time. *Palaeogeography, Palaeoclimatology, Palaeoecology*, 87(1–4), 373–409. https://doi.org/10.1016/0031-0182(91)90142-E
- Stanley, S. M. (2016). Estimates of the magnitudes of major marine mass extinctions in earth history. Proceedings of the National Academy of Sciences of the United States of America, 113(42), E6325–E6334. https://doi.org/10.1073/pnas.1613094113
- Summons, R. E., & Powell, T. G. (1987). Identification of aryl isoprenoids in source rocks and crude oils: Biological markers for the green sulphur bacteria. *Geochimica et Cosmochimica Acta*, 51(3), 557–566. https://doi.org/10.1016/0016-7037(87)90069-X
- Sun, Y. (2024). Dynamics of nutrient cycles in the Permian–Triassic oceans. Earth-Science Reviews, 258, 104914. https://doi.org/10.1016/j.earscirev.2024.104914
- Sun, Y., Farnsworth, A., Joachimski, M. M., Wignall, P. B., Krystyn, L., Bond, D. P. G., et al. (2024). Mega El Niño instigated the end-Permian mass extinction. *Science*, 385(6714), 1189–1195. https://doi.org/10.1126/science.ado2030
- Sun, Y. D., Zulla, M. J., Joachimski, M. M., Bond, D. P. G., Wignall, P. B., Zhang, Z. T., & Zhang, M. H. (2019). Ammonium ocean following the end-Permian mass extinction. Earth and Planetary Science Letters, 518, 211–222. https://doi.org/10.1016/j.epsl.2019.04.036
- Twitchett, R. J., & Barras, C. G. (2004). Trace fossils in the aftermath of mass extinction events. In D. McIlroy (Ed.) *The application of ichnology to palaeoenvironmental and stratigraphic analysis* (Vol. 228, pp. 397–418). Geological Society, London, Special Publications. https://doi.org/10.1144/GSL.SP.2004-228.01.18
- Uchman, A., Hanken, N. M., Nielsen, J. K., Grundvåg, S.-A., & Piasecki, S. (2016). Depositional environment, ichnological features and oxygenation of Permian to earliest Triassic marine sediments in central Spitsbergen, Svalbard. *Polar Research*, 35(1), 24782. https://doi.org/10.3402/polar.v35.24782
- Vandier, F., Tourte, M., Doumbe-Kingue, C., Plancq, J., Schaeffer, P., Oger, P., & Grossi, V. (2021). Reappraisal of archaeal C<sub>20</sub>-C<sub>25</sub> diether lipid (extended archaeol) origin and use as a biomarker of hypersalinity. *Organic Geochemistry*, 159, 104276. https://doi.org/10.1016/j.orggeochem. 2021.104276
- Wong, J. C., Raven, J. A., Aldunate, M., Silva, S., Gaitán-Espitia, J. D., Vargas, C. A., et al. (2023). Do phytoplankton require oxygen to survive? A hypothesis and model synthesis from oxygen minimum zones. *Limnology & Oceanography*, 68(7), 1417–1437. https://doi.org/10.1002/lno.
- Worsley, D. (2008). The post-Caledonian development of Svalbard and the western Barents Sea. *Polar Research*, 27(3), 298–317. https://doi.org/10.1111/j.1751-8369.2008.00085.x
- Wu, J., Chu, D., Luo, G., Wignall, P. B., Algeo, T. J., & Xie, S. (2023). Stepwise deforestation during the Permian-Triassic boundary crisis linked to rising temperatures. Earth and Planetary Science Letters, 620, 118350. https://doi.org/10.1016/j.epsl.2023.118350
- Xiang, L., Zhang, H., Schoepfer, S. D., Cao, C., Zheng, Q., Yuan, D., et al. (2020). Oceanic redox evolution around the end-Permian mass extinction at Meishan, South China. *Palaeogeography, Palaeoclimatology, Palaeoecology, 544*, 109626. https://doi.org/10.1016/j.palaeo. 2020.109626
- Xie, S., Algeo, T. J., Zhou, W., Ruan, X., Luo, G., Huang, J., & Yan, J. (2017). Contrasting microbial community changes during mass extinctions at the middle/late Permian and Permian/Triassic boundaries. *Earth and Planetary Science Letters*, 460, 180–191. https://doi.org/10.1016/j.epsl. 2016.12.015
- Xie, S., Pancost, R. D., Huang, J., Wignall, P. B., Yu, J., Tang, X., et al. (2007). Changes in the global carbon cycle occurred as two episodes during the Permian-Triassic crisis. *Geology*, 35(12), 1083–1086. https://doi.org/10.1130/G24224A.1
- Xie, S., Pancost, R. D., Wang, Y., Yang, H., Wignall, P. B., Luo, G., et al. (2010). Cyanobacterial blooms tied to volcanism during the 5 m.y. Permo-Triassic biotic crisis. *Geology*, 38(5), 447–450. https://doi.org/10.1130/G30769.1
- Yin, H., Zhang, K., Tong, J., Yang, Z., & Wu, S. (2001). The global stratotype section and point (GSSP) of the Permian-Triassic boundary. Episodes Journal of International Geoscience, 24(2), 102–114. https://doi.org/10.18814/epiiugs/2001/v24i2/004
- Zhang, F., Shen, S., Cui, Y., Lenton, T. M., Dahl, T. W., Zhang, H., et al. (2020). Two distinct episodes of marine anoxia during the Permian-Triassic crisis evidenced by uranium isotopes in marine dolostones. *Geochimica et Cosmochimica Acta*, 287, 165–179. https://doi.org/10.1016/j.gca.2020.01.032
- Zhang, Y., Wen, H., Zhu, C., Fan, H., & Cloquet, C. (2018). Cadmium isotopic evidence for the evolution of marine primary productivity and the biological extinction event during the Permian-Triassic crisis from the Meishan section, South China. Chemical Geology, 481, 110–118. https:// doi.org/10.1016/j.chemgeo.2018.02.005
- Zuchuat, V., Sleveland, A. R. N., Twitchett, R. J., Svensen, H. H., Turner, H., Augland, L. E., et al. (2020). A new high-resolution stratigraphic and palaeoenvironmental record spanning the end-Permian mass extinction and its aftermath in central Spitsbergen, Svalbard. *Palaeogeography*, *Palaeoclimatology*, *Palaeoecology*, 554, 109732. https://doi.org/10.1016/j.palaeo.2020.109732

BUCHWALD ET AL. 15 of 15